Structures and Micelle Locations of the Nonlipidated and Lipidated C-Terminal Membrane Anchor of 2`,3`-Cyclic Nucleotide-3`-phosphodiesterase†

ARTICLE *in* BIOCHEMISTRY · DECEMBER 2007

Impact Factor: 3.02 · DOI: 10.1021/bi701474t

Structures and Micelle Locations of the Nonlipidated and Lipidated C-Terminal Membrane Anchor of 2′,3′-Cyclic Nucleotide-3′-phosphodiesterase†

Cinzia Esposito,‡ Mario Scrima,‡ Alfonso Carotenuto,§ Annamaria Tedeschi,‡ Paolo Rovero,|| Gerardino D'Errico,⊥ Anna Maria Malfitano,‡ Maurizio Bifulco,‡ and Anna Maria D'Ursi*,‡

Department of Pharmaceutical Sciences, University of Salerno, I-84084 Fisciano, Italy, Department of Pharmaceutical and Toxicological Chemistry, University of Naples "Federico II", I-80131 Naples, Italy, Laboratory of Peptide and Protein Chemistry and Biology, University of Florence, I-50019 Sesto Fiorentino, Italy, and Department of Chemistry, University of Naples "Federico II", I-80126 Naples, Italy

Received July 25, 2007; Revised Manuscript Received October 18, 2007

ABSTRACT: 2,3′-Cyclic nucleotide-3′-phosphodiesterase (CNP) is a myelin-associated protein, an enzyme abundantly present in the central nervous system of mammals and some vertebrates. *In vitro*, CNP specifically catalyzes the hydrolysis of 2′,3′-cyclic nucleotides to produce 2′-nucleotides, but the physiologically relevant *in vivo* substrate is still unknown. Recently, it was found that CNP is a possible linker protein between microtubules and the plasma membranes. Since CNP is modified post-translationally by an isoprenylation process at its C terminus, the prenylation is hypothesized to be a requisite process, which permanently anchors CNP to the plasma membrane. This study investigates the molecular mechanism of the interaction between CNP and the plasma membrane, proposing a general model to interpret the structural bases of prenylated proteins binding to the membrane. A 13 residue, C-terminal CNP fragment, C13, was demonstrated to be directly responsible for CNP membrane anchoring. C13 and its lipidated derivative (LIPO-C13) were subjected to conformational analysis in membrane mimetic environments, by means of CD and NMR spectroscopies. The orientation of C13 in relation to the membrane was investigated by NMR and EPR spin labeling studies. Our structural investigation shows that the presence of the lipidic tail is essential for the peptide to be folded and correctly positioned on the membrane surface. A general model is proposed in which the post-translational lipidation is an important biomolecular trick to enlarge the hydrophobic surface and to enable the contact of the protein with membrane.

2,3′-Cyclic nucleotide 3′-phosphodiesterase (CNP)[1] is a myelin-associated enzyme abundantly present in the central nervous system of mammals and some vertebrates. It is one of the earliest myelin-related proteins to be expressed in differentiating oligodendrocytes and Schwann cells (*1*). Although its biological function is still unknown, numerous independent studies suggest a role for this protein in the migration and/or expansion of membranes during myelination (*2*). CNP is expressed as two isoforms with a molecular mass of around 46 kDa (CNP1) and 48 kDa (CNP2), differing only by a 20-amino acid extension at the N-terminus (*2*, *3*). Both isoforms are modified by isoprenylation at their C terminus (*4*) and the protein is found attached to the plasma membrane of various cells, provided both prenylation and palmitoylation modifications have occurred. The association of CNP with the cytoskeleton was also suggested by Braun at al (*5*) and we previously demonstrated that CNP is firmly associated with tubulin from brain tissue and thyroid cells acting as a membrane microtubule-associated protein (MAP) in promoting microtubule assembly (*5*−*7*).

The CNP region responsible for the interaction with the plasma membrane is a segment consisting of 13 amino acids located in the C-terminus of the protein (*6*, *7*). CNP lacking this sequence loses both the membrane and tubulin binding properties. Thus C13 can be considered a bridge sequence which includes both membrane and tubulin anchoring sites. C13 includes a CAAX ("C" refers to the cysteine, "A" to any aliphatic amino acid, and "X" to any amino acid)

† We thank the Associazione Educazione e Ricerca Medica Salernitana (ERMES) for supporting our studies.

* Corresponding author. Anna Maria D'Ursi, Dipartimento di Scienze Farmaceutiche, Universita' di Salerno, Via Ponte don Melillo 84084 Fisciano (Salerno), Italy. Phone: 39-089/969748. Fax: 39-089/969602. E-mail: dursi@unisa.it.

‡ University of Salerno.

§ Department of Pharmaceutical and Toxicological Chemistry, University of Naples "Federico II".

|| University of Florence.

⊥ Department of Chemistry, University of Naples "Federico II".

[1] Abbreviations: CNP, 2′,3′-cyclic nucleotide 3′-phosphodiesterase; MAP, microtubule-associated protein; MBP, myelin basic protein; SDS, sodium dodecyl sulfate; DOPC, 1,2-dioleoyl-*sn*-glycero-3-phosphocholine; DOPG, 1,2-dioleoyl-*sn*-glycero-3-[phospho-*rac*-(1-glycerol)]; DPC, dodecylphosphocholine; Fmoc, 9-fluorenylmethoxycarbonyl; HBTU, *O*-(benzotriazol-1-yl)-1,1,3,3-tetramethyluronium hexafluorophosphate; HOBt, 1-hydroxybenzotriazole; AOD, 2-aminooctadecanoic acid; DMF, *N*,*N*-dimethylformamide; tBu, *tert*-butyl; TFA, trifluoroacetic acid; TIS, triisopropylsilane; 5-DSA, 5-DOXYL-stearic acid; 16-DSA, 16-DOXYL-stearic acid; RT, room temperature; ESI-MS, electrospray ionization-mass spectroscopy; NMR, nuclear magnetic resonance; COSY, correlated spectroscopy; TOCSY, total correlated spectroscopy; NOESY, nuclear Overhauser effect spectroscopy; EPR, electron paramagnetic resonance. Abbreviations used for amino acids and designation of peptides follow the rules of the IUPAC-IUB Commission of Biochemical Nomenclature in *J. Biol. Chem.* 1972, *247*, 977-983. Amino acid symbols denote L-configuration unless indicated otherwise.

10.1021/bi701474t CCC: $40.75
Published on Web 12/13/2007

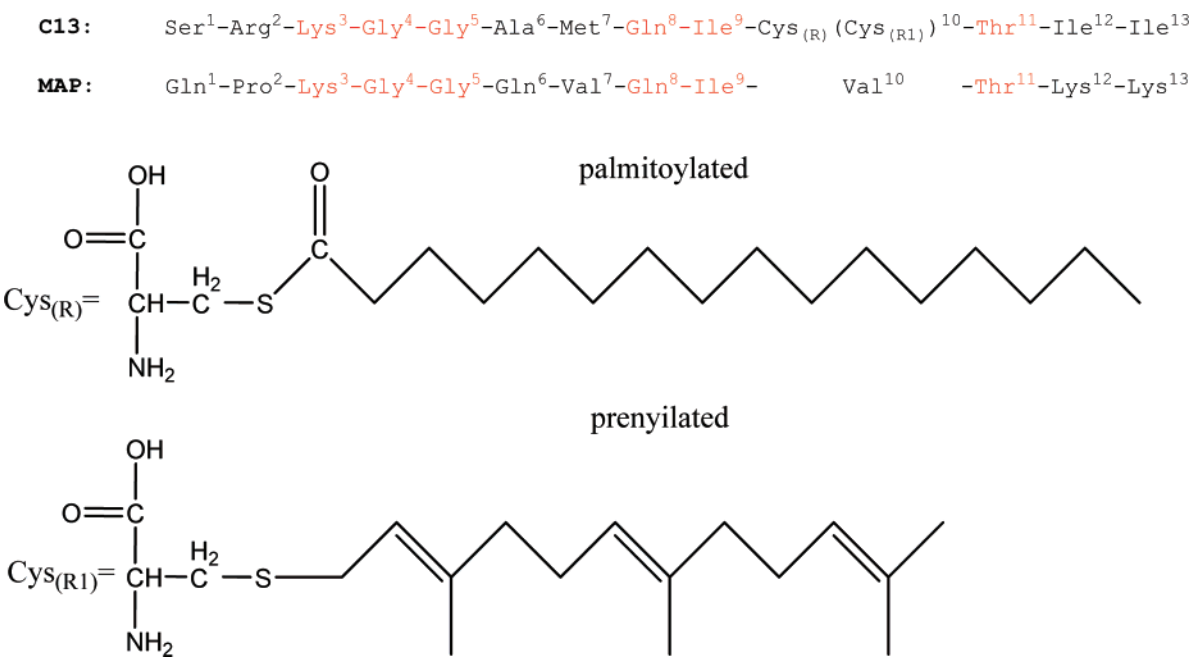

FIGURE 1: Sequence alignment of CNP C13-segment and tubulin-binding domain of MAP2. Amino acid sequence of C13, Cys(R), Cys-(R1) represents post-translational palmitoylation or prenylation.

consensus motif which *in vivo* is an isoprenylation site (*8*−*10*) and is essential to membrane anchoring. Hence, *in vivo* CNP in correspondence with the C13 sequence is both prenylated and palmitoylated (*11*), providing hydrophobic sites for membrane binding (*4*, *11*−*12*). CNP shares this property with ras oncoproteins and their relatives, some G-proteins, and nuclear lamins (*11*−*15*). On the other hand, in correspondence with the C13 sequence, it exhibits a significant homology with the tubulin-binding domain of MAP2 (view Figure 1). Accordingly, C13 was proven to be endowed with microtubule-associated protein (MAP)-like properties exerting a pivotal role for microtubule assembly (*7*, *16*, *17*).

CNP was involved in aberrant myelination (*19*, *20*), in Down syndrome, in Alzheimer's disease, and multiple sclerosis (*21*−*26*); the disruption of the CNP gene was proven to cause hydrocephalus and premature death. These CNP bioactivities bring to mind a similarity of CNP to other proteins implicated in neurodegenerative diseases. In particular a malfunction of CNP as a membrane-interacting peptide can be determinant to producing the reduction in the membrane plasticity which is a feature of many neurodegenerative diseases.

Therefore, the role of CNP as a molecular linker between membrane and intracellular effectors and additionally its implication as a protein involved in neuronal diseases suggest that CNP plays a vital role for cell life and in this regard can be considered an emerging target for potential therapeutic use in cancer as well as in neurodegenerative diseases.

Here we report the synthesis and the conformational analysis of the membrane−tubulin bridge peptide C13. The study was performed in parallel, also on C13- lipidated derivative LIPO-C13, in which 2-aminooctadecanoic acid replaces the Cys^{10} residue. To analyze the structural features of C13 as a membrane bound peptide, C13 and LIPO-C13 were extensively investigated by means of NMR, EPR, and CD spectroscopies in different membrane-mimicking environments. For technical reasons, high-resolution NMR studies were performed in SDS and DPC micelle solutions. Nevertheless, to validate the data in a more significant biomimetic system, CD data were recorded in DOPC and DOPG multilamellar vesicles. The comparison of C13 and LIPO-C13 structural features allowed evaluation of the potential of the lipidic tail, and more specifically, of CNP prenylation, to affect the conformational propensity of CNP and its membrane binding properties (*5*, *6*, *18*).

MATERIALS AND METHODS

Peptide Synthesis. C13 (SRKGGAMQICTII) and LIPO-C13, containing 2-aminooctadecanoic acid (AOD) in the C-terminus (SRKGGAMQI(AOD)TII), were manually synthesized on solid phase, using standard Fmoc/tBu chemistry. The TentaGel S RAM (capacity of 0.20 mmol/g) resin was purchased from Fluka (Sigma Aldrich, Italy). After deprotection of the Fmoc group with 30% of piperidine in DMF, the amino acids in 4 fold excess were coupled to the growing peptide chain, using DMF solution with an equimolar amount of HOBt and HBTU. For the synthesis of LIPO-C13, the Fmoc-L-2-aminoctadecanoic acid (Fmoc-AOD-OH), from EspiKem (Italy), was introduced by double coupling as a standard amino acid. All the reagents were from Novabiochem (France) or Sigma Aldrich (Italy). Other solvents and reagents used in peptide synthesis were obtained from Sigma (Italy) or Carlo Erba (Italy) and used without further purification. Peptide−resin cleavage and side-chain deprotection reactions were carried out in 95% TFA, 2.5% water, and 2.5% of TIS. After filtration to remove the resin followed by cold ether precipitation, the crude peptides were recovered.

HPLC Purification. Analytical HPLC was carried out on a System Gold 125s model (Beckmann Coulter) equipped with a UV166 detector. Preparative HPLC was carried out on a Waters 600E system controller equipped with a 486 UV detector. A Jupiter (Phenomenex) C18 column (25 × 4.6 cm, 5 μm, 300 Å pore size) was used for analytical runs

and a Vydac C18 column (25 × 10 cm, 5 μm, 300 Å pore size) for peptide purification. Analytical separations were performed with eluant A: 0.1% TFA/water, eluant B: 0.1% TFA/acetonitrile, using a linear gradient from 5% to 65% B over 20 min, flow rate: 1 mL/min, detection: UV, 210 nm, t_R: 12.2 min, HPLC purity: 64% (expressed as peak height %). The main peak was isolated by preparative HPLC, using a Vydac C18 column (2.2 × 25 cm): eluants A and B as indicated above, gradient from 15% to 44% B over 120 min, flow 4 mL/min, UV detection at 210 nm.

Mass Spectral Analysis. The two peptides were characterized on a Finningan LCQ-Deca ion trap instrument equipped with an electrospray source (LCQ Deca Finnigan, San José. CA). Samples were directly infused into the ESI source by using a syringe pump at the flow rate of 5 μL/min. Data were analyzed with Xcalibur software.

Circular Dichroism. Samples for CD spectroscopy were prepared by dissolving C13- and LIPO-C13 peptides in water to a concentration of 0.1 mM. The pH was adjusted to 5.6 using phosphate buffer. Samples for CD in micelle solutions were prepared using SDS and DPC surfactants in 10 fold excess concentration as compared to their cmc (*27*, *28*).

Liposomes for CD spectroscopy were prepared by dissolving DOPC and DOPG phospholipids in chloroform/methanol (50/50). The solvent was then removed with nitrogen evaporation and under high vacuum at room temperature for at least 1 h. The dry lipid films were resuspended in deionized water containing 0.01 mM peptides. The vesicles were prepared at a temperature higher than the gel−liquid crystal transition temperature. The suspension was then vortexed to produce the desired liposomes. The liposome samples were prepared to have a peptide/phospholipid molar ratio of 1/4.

All CD spectra were recorded using a JASCO J810 spectropolarimeter at room temperature, with a cell of 1 mm path length. The CD spectra were recorded using a measurement range from 260 to 190 nm, 1 nm bandwidth, four accumulations, and 10 nm/min scanning speed. All the spectra were analyzed, subtracted by blanks, and finally corrected by smoothing. The estimation of the secondary structure composition was carried out using the algorithm K2D by Dicroweb (*29*).

NMR Spectroscopy. NMR samples were prepared by dissolving the appropriate amount of C13 and LIPO-C13 in 0.5 mL of an aqueous mixture H_2O/D_2O (90/10) solution to obtain a 1.5 mM peptide concentration, in the absence or in the presence of SDS-d_{25} and DPC-d_{38}. Deuterated surfactants were added at a 10-fold concentration compared to the cmc. The NMR samples were prepared to have a peptide/surfactant molar ratio of 1/100 (*30*, *31*).

NMR spectra were collected on a Bruker DRX-600 spectrometer, at 300 K. One-dimensional (1D) NMR spectra were recorded in the Fourier mode with quadrature detection, and the water signal was suppressed by low-power selective irradiation in the homogated mode. DQF-COSY, TOCSY, and NOESY experiments were run in the phase-sensitive mode using quadrature detection in ω1 via time-proportional phase increases of initial pulse (*32*−*35*). Data block sizes were 2048 addresses in t2 and 512 equidistant t1 values. Before Fourier transformation, the time domain data matrices were multiplied by shifted $\sin^2$ functions in both dimensions. A mixing time of 70 ms was used for the TOCSY experiments. NOESY experiments were run with mixing times in the range of 100−250 ms. The qualitative and quantitative analysis of DQF-COSY, TOCSY, and NOESY spectra was achieved using SPARKY software (*36*).

NMR and EPR Experiments in the Presence of Spin-Probes. For NMR experiments, two different solutions of 5-DSA and 16-DSA spin-probes were prepared using methanol-d_4 as solvent. Spin-probes were added to deuterated DPC-d_{38} micellar solutions of C13 and LIPO-C13 peptides in a concentration ratio corresponding to spin probe/micelle 1:1.

In the case of EPR experiments, the samples were prepared by weight at a surfactant concentration 10 times higher than cmc and a spin-probe concentration equal to 0.5 mM. The concentration of the peptide, if present, was 1 mM. The samples were deoxygenated and successively sealed in 1.00 mm i.d. quartz capillaries in a nitrogen atmosphere. EPR spectra were obtained using a Bruker ELEXYS e500 X-band spectrometer. The instrument parameters were as follows: modulation amplitude 0.16 G to avoid signal over modulation, time constant 1.28 ms, receiver gain 60 dB, microwave power 2 mW (20 dB) to prevent saturation effects. All measurements were performed at room temperature. The isotropic nitrogen hyperfine coupling constant and the correlation time of the spin probes were obtained from the experimental spectra as described in a previous work (*37*).

Refinement of the Structure by Molecular Dynamics Calculations. Peak volumes of NOESY spectra at 150 ms were translated into upper distance bounds with the routine CALIBA of the DYANA software (*38*). The requisite pseudoatom corrections were applied for nonstereospecifically assigned protons at prochiral centers and for the methyl group. After redundant and duplicated constraints were discarded, an ensemble of 100 structures was generated by the standard protocol of simulated annealing in torsion angle space implemented in DYANA (using 6000 steps). The number of NOE-based distance restraints used with DYANA calculation for C13 and LIPO-C13 in SDS was 130 and 164, respectively; NOE-based restraints for the calculation of C13 and LIPO-C13 in DPC micelles were 190 and 212. respectively. No dihedral angle restraints and no hydrogen bond restraints were applied. The best 20 structures, which had low target function values (0.83−1.19) and small residual violations (maximum violation = 0.38 Å), were refined by in vacuo minimization in the AMBER 1991 force field, using the SANDER program of the AMBER 5.0 suite (*39*). To mimic the effect of solvent screening, all net charges were reduced to 20% of their real value, and moreover a distance-dependent dielectric constant ($\epsilon = r$) was used. The cutoff for nonbonded interactions was 12 Å. The NMR-derived upper bounds were imposed as semiparabolic penalty functions, with force constants of 16 kcal/mol Å^2, and the function was shifted to linear when the violation exceeded 0.5 Å. The best 10 structures after minimization had AMBER energies ranging from −441.4 to −391.1 kcal/mol. The final structures were analyzed using the Insight 98.0 program (Molecular Simulations, San Diego, CA) (*40*).

RESULTS

Choice of the Solvent. CD and NMR experiments were performed in zwitterionic DPC and negatively charged SDS

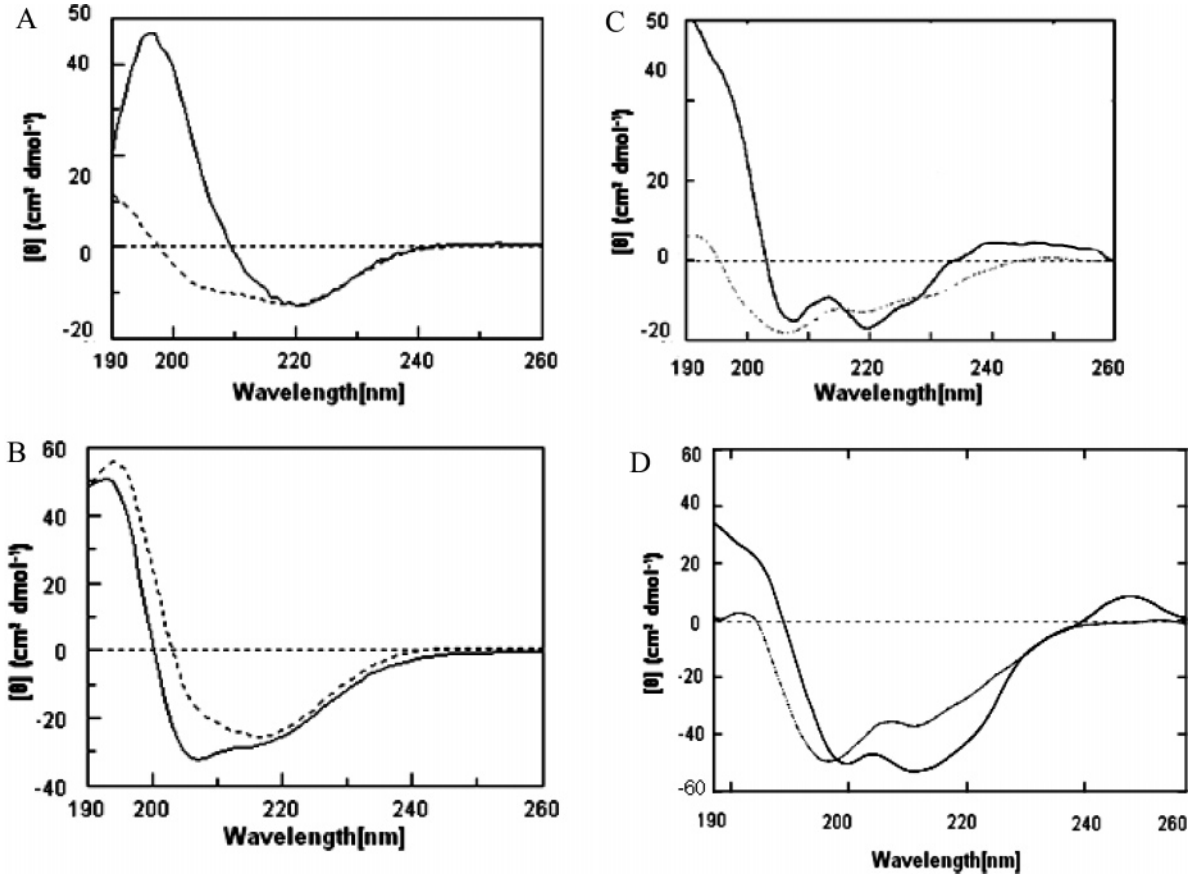

FIGURE 2: (A, B) CD spectra of C13 (A) and LIPO-C13 (B) in the presence of SDS (continuous line) and DPC micelles (dotted line). (C, D) CD spectra of C13 (C) and LIPO-C13 (D) in the presence of DOPG (continuous line) and of DOPC (dotted line) multilamellar vesicles.

micelles. Additional CD spectra were recorded in negatively charged DOPG and zwitterionic DOPC multilamellar vesicles.

Solutions containing micellar aggregates, are frequently used as membrane mimicking systems, for the high-resolution NMR analysis of short peptides acting at the cell membrane interface. Micelle solutions are composed of surfactants, such as DPC or SDS, at a concentration higher than their cmc. These surfactants form spherical aggregates where the polar head-groups are located on the surface and the hydrophobic tail in the core. Micelle solutions are suitable systems for NMR analysis, since, thanks to their short rotational correlation time, they produce good quality proton spectra (*30*). However micelles are very simple models, very different from plasma membranes in complexity and variability. In order to validate, in a more reliable biomimetic medium, the results derived from SDS and DPC experiments, we recorded CD spectra of C13 and LIPO-C13 in DOPG and DOPC vesicles. DOPG and DOPC are anionic and zwitterionic phospholipids, able to aggregate, forming multilamellar vesicles characterized by negatively charged and zwitterionic surfaces, respectively (*27*, *28*).

CD Spectroscopy. Figure 2 shows CD spectra of C13 (Figure 2A) and LIPO-C13 (Figure 2C), in SDS (continuous line) and in DPC (dotted line) micellar solutions. The comparison of CD curves for C13 in SDS and DPC micelles indicates a different conformational behavior of the peptide in the two micellar systems. The quantitative interpretation of C13 and LIPO-C13 CD spectra (Table 1A), using K2D algorithm from DichroWeb (*29*), indicates that C13 in SDS micelles assumes a prevalence of extended (45%) and random coil (30%) conformations, whereas in DPC a significant percentage of turn-helical structures is observable.

Table 1: Quantitative Estimation (%) of CD Spectra Relative to C13 and LIPO-C13 in (A) SDS and DPC Micelles and (B) DOPG and DOPC Vesicles Using K2D Algorithm from DichroWeb (*29*) Website

	helix	strand	turns	unordered
A. In SDS and DPC Micelles				
C13 in DPC	40	10	20	30
LIPO-C13 in DPC	60	5	10	25
C13 in SDS	10	45	15	30
LIPO-C13 in SDS	30	5	20	45
B. In DOPG and DOPC Vesicles				
C13 in DOPC	70	0	10	20
LIPO-C13 in DOPC	76	3	0	21
C13 in DOPG	15	30	15	40
LIPO-C13 in DOPG	16	0	36	49

CD spectra of LIPO-C13 show that the lipopeptide is less perceptive to the nature of the micelle as compared to C13. Indeed the CD spectra of LIPO-C13 in SDS and DPC micelles are comparable. Accordingly, the quantitative estimation of LIPO-C13 CD spectra in SDS and DPC micelles (Table 1A) indicates similar values of about 50% of turn-helical structures.

Figure 2B and 2D show CD spectra of C13 and LIPO-C13 in DOPG (continuous line) and in DOPC (dotted line) vesicles. A general increasing of helical content is observable for both C13 and LIPO-C13 in the vesicle systems as compared to the micellar solutions. The comparison of C13 CD spectra in DOPG and DOPC vesicles demonstrates a clear difference in the shape of the curves, confirming the

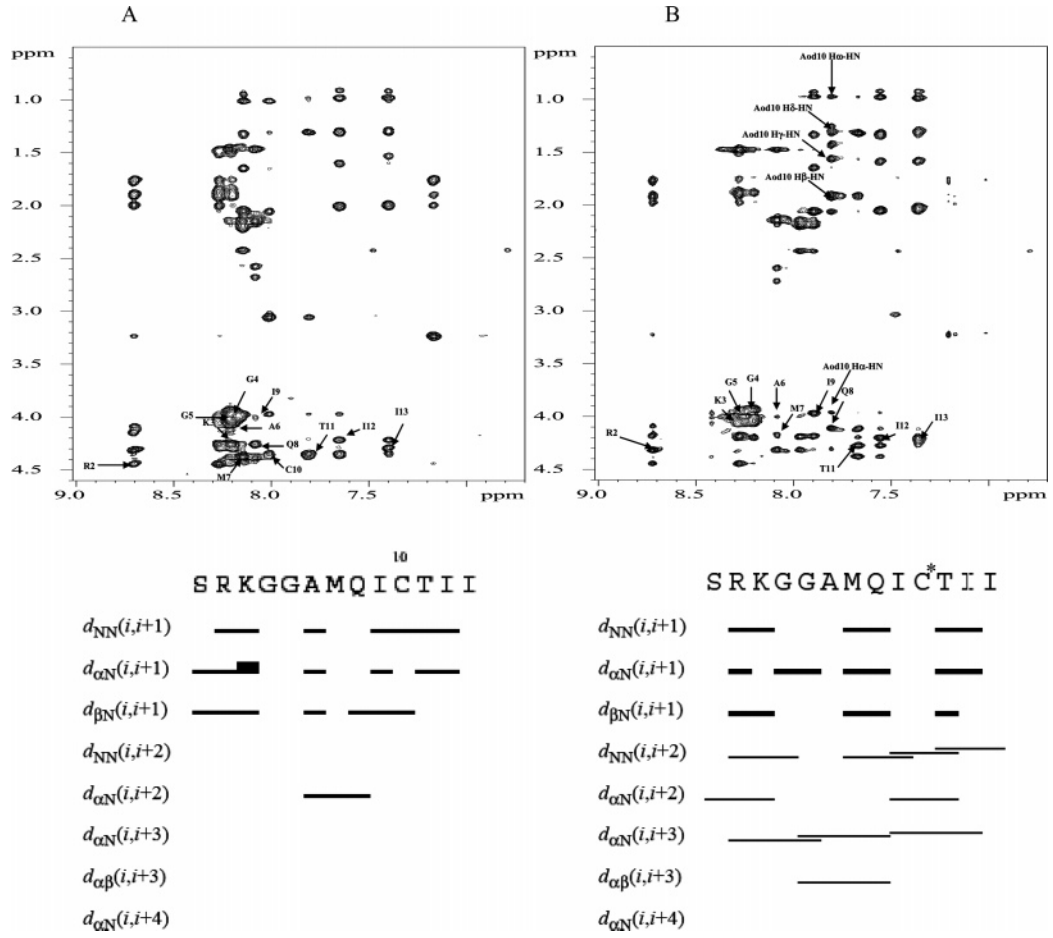

FIGURE 3: NH−CHα NOESY spectra of C13 (A) and LIPO-C13 (B) in SDS micelles. The spectra were recorded at 600 MHz, 300 K, 150 ms mixing time. At bottom of each NOESY spectra, the relative bar diagrams are reported, summarizing the sequential and medium range NOE connectivities.

high sensitivity of C13 to the membrane composition. The same comparison made for LIPO-C13 shows significant similarity between the spectra, suggesting that the lipo derivative is less responsive to the electrostatic nature of the vesicle surface. A quantitative interpretation of CD spectra confirms these results as reported in Table 1B.

NMR Analysis. A whole set of 1D and 2D proton spectra were recorded in SDS and in DPC micellar solutions. To check the absence of self-aggregation, spectra were acquired in the peptide concentration range of 0.5−15 mM. No significant changes were observed in the distribution and in the shape of the ^{1}H resonances, indicating that no aggregation phenomena occurred in this concentration range. Complete assignments of the proton spectra of C13 and LIPO-C13 in micellar environments (see Supporting Information) were achieved by the standard Wüthrich procedure (*41*). Analysis of 2D spectra was performed using the SPARKY software package (*36*).

The one-dimensional NMR spectra of C13 and LIPO-C13 in micelles show a significant spreading (from 7.2 to 9.0) of the amide signals for both the peptides as compared to the NH dispersion typical of random coil conformations. This suggests that the interaction of the peptides with the micellar surface is important to stabilize ordered conformation over flexible disordered ones.

The amide plot (data not shown) summarizing the secondary shifts of amide protons for C13 and LIPO-C13 in SDS and DPC micelles shows that although the NH chemical shifts are significantly different than NH values of random coil peptides, no periodicity is observable, according with the absence of amphipathic structure (*42*).

The analysis CHα chemical shifts for C13 and LIPO-C13 in SDS and DPC micelles shows a remarkable upfield shift compared to the standard values reported for random coil conformations. According to the Chemical Shift Index (CSI) grouping of four (not necessarily consecutive) "−1s" is needed to define turn-helix conformations. Regions characterized by nonconsecutive "0s" or "1s" are designated as coils (*43*). C13 and LIPO-C13 in micelles show "−1s" values of chemical shift (see Supporting Information); this is suggestive of the presence of turn-helix conformation.

Figure 3 shows the low field region and the NOE connectivities of NOESY spectra of C13 (Figure 3A) and LIPO-C13 (Figure 3B) in SDS micelles. The NOE patterns for the two peptides in SDS micelles are substantially different. In particular, in accordance with the nonappearance of medium range (i, $i + 2$) and (i, $i + 3$) connectivities, C13 shows a conformational preference for extended unfolded conformations. On the contrary, critical αN(i, $i + 3$) and αβ(i, $i + 3$) medium range connectivities suggest a detectable conformational preference of LIPO-C13 to assume ordered conformations involving in particular the residues Gly^5-Glu^8. A model of the conformational preferences of LIPOC13 in SDS micelles was calculated using DYANA software, on

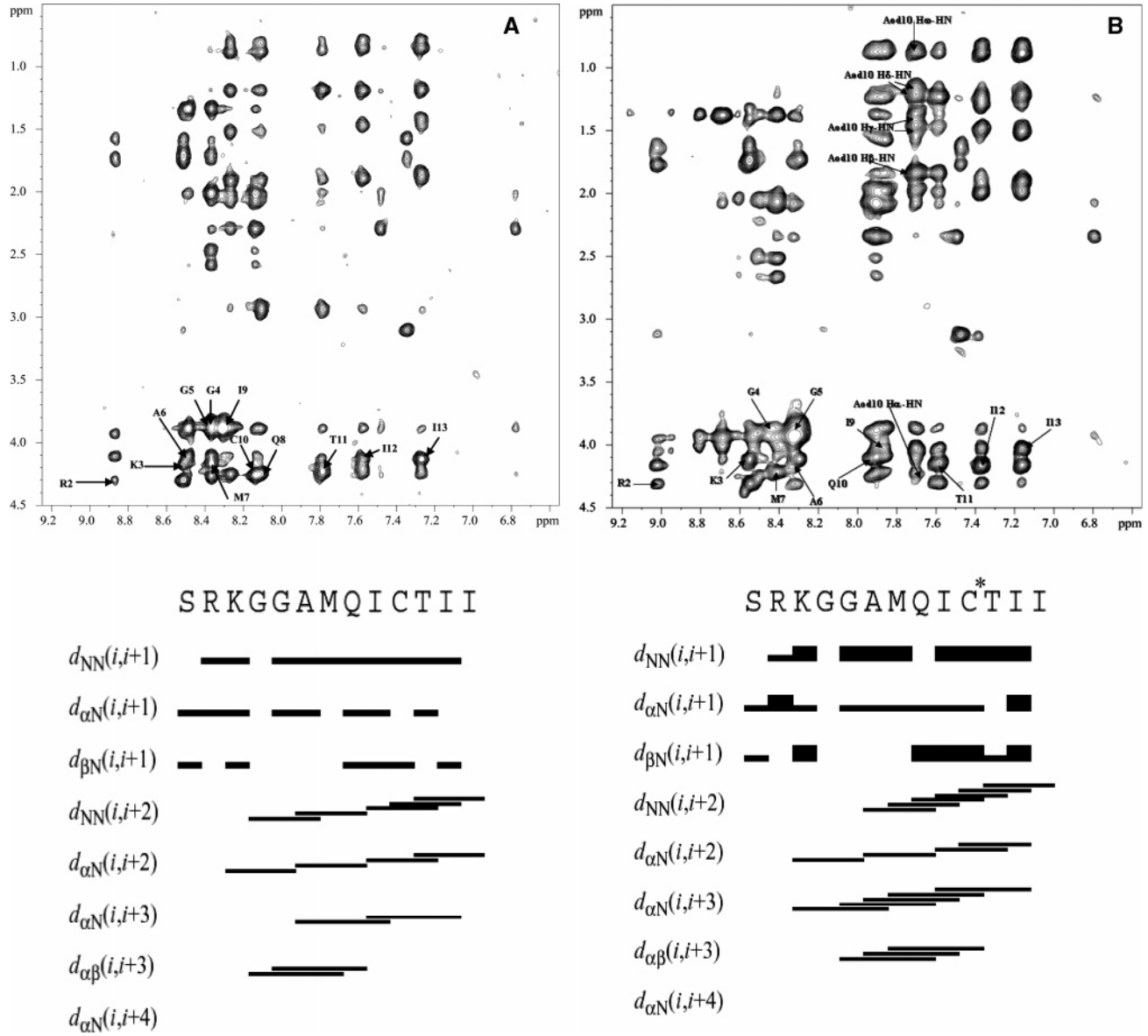

FIGURE 4: NH−CHα NOESY spectra of C13 (A) and LIPO-C13 (B) in DPC micelles. The spectra were recorded at 600 MHz, 300 K, 150 ms mixing time. At bottom of each NOESY spectra, the relative bar diagrams are reported, summarizing the sequential and medium range NOE connectivities.

the basis of NOE data. 3D structure calculation of C13 in SDS micelles was not achievable due to the low number and the low intensity of NOEs.

NH−CHα NOESY spectra and NOE correlations relative to the C13 and LIPO-C13 in DPC micelles are summarized in Figure 4.

Several medium range connectivities are observable for C13 in DPC micelles: in particular the contacts relative to $CH_\alpha N_H(i, i + 2)$ NOE cross-peak between residues Lys^3-Gly^5, Gly^5-Met^7, Ala^8-Cys^{10}, and Cys^{10}-Ile^{12}; furthermore, intense $CH_\alpha CH2_b$ (i, $i + 3$) NOE cross-peaks involving residues Lys^3-Ala^6 and Gly^4-Met^7 are detectable (Figure 4A). The calculation of 3D structure (Figure 5A) using DYANA software on the basis of these NOE data demonstrated the presence of a type I β-turn conformation centered on the residues Ala^6-Met^7, whereas a type II β-turn conformation is centered on the residues Thr^{11}-Ile^{12} (Figure 5A). On the other hand, the N-terminal region of C13 in DPC micelles does not exhibit any regular NOE pattern, suggesting the prevalence, in this region, of flexible, extended structures.

NOE data relative to LIPO-C13 in DPC micelles indicated a regular pattern of sequential and medium range NOEs along the whole sequence (Figure 4B). The structure calculation using DYANA software was consistent with the presence of a regular α-helix encompassing the residues from Ala^2 to Ile^{12} (Figure 5B). Differently from C13, no violation higher than 0.1 Å was observed in the helical region for LIPO-C13, thus indicating the absence of any conformational averaging in the micelle-bound structure of the lipidated peptide. The best NMR structures were subjected to molecular dynamic calculation to assess the stability of the backbone and to explore the mobility of the side chains. The computation of the Van der Waals surfaces (Figure 6) relative to C13 and LIPO-C13 DPC-bound conformations were carried out using the MOLMOL program (*44*). The surfaces show narrow, polar, charged regions in the N-terminal portion of the molecules, whereas large hydrophobic shells are evident at C terminus of the peptides. The comparison

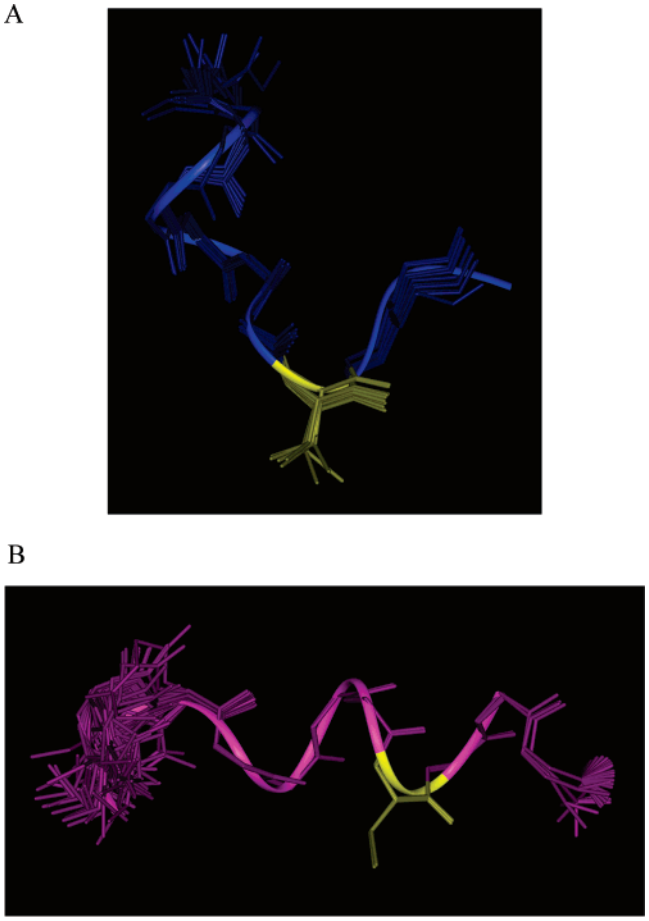

FIGURE 5: NMR structure bundles of C13 (A) and LIPO-C13 (B) in DPC micelles. The structures are overlapped on the backbone heavy atoms of the residues Ala^{6}-Ile^{12} for C13 and Gly^{4}-Ile^{12} for LIPO-C13.

of C13 and LIPO-C13 demonstrates a consistent amplification of the hydrophobic area in LIPO-C13 due to the presence of the lipidated chain.

Complementary NMR and EPR Methods by Spin-Label Studies. To investigate the positioning of C13 and LIPO-C13 relative to the surface and interior of the micelles, we subsequently introduced 5-DSA and 16-DSA as molecular spin-probes in the micellar systems.

Unpaired electrons lead to dramatically accelerated longitudinal and transverse relaxation rates of protons in spatial proximity *via* highly efficient spin-electron relaxation. Generally, if the peptide penetrates the membrane in the neighborhood of the site where the NO moiety is solubilized, the presence of the unpaired electron induces an increase in peptide nuclear relaxation rates. It has been shown that these paramagnetic probes are able to induce a broadening of the NMR signals and a decrease in resonance intensities for residues close to the surface (5-DSA) or deeply buried inside the micelle (16-DSA), respectively (*45*, *46*).

1D and 2D TOCSY spectra of C13 and LIPO-C13 were recorded in DPC micellar solution in the presence and absence of 5-DSA and 16-DSA, respectively, keeping all other conditions constant. The comparison of the data acquired in the presence and absence of spin probes shows that the peptides are affected by the presence of the spin probes.

Figure 7 shows the overlapping of the NH/CHα TOCSY spectra of LIPO-C13 in DPC micelles in the presence and in the absence of 5-DSA (Figure 7A) and 16 DSA (Figure 7B), respectively. LIPO-C13 in DPC micelles was perturbed by 5-DSA with a general decrease of cross-peak intensities. In particular the NH/CHα relative to the residues from Ala^{6} to AOD^{10} almost annulled their intensities; on the other side the NH/CHα relative to Lys^{3}, Thr^{11}, Ile^{12}, Ile^{13} were less dramatically affected by the presence of the spin probe. The effect of 16-DSA was generally less evident as compared to that of 5-DSA; in particular the signals relative to the C-terminal residues showed a general decrease of intensity. Figure 7C shows the overlapping of the NH/CHα TOCSY spectra of C13 in DPC micelles recorded in the absence and in the presence of 5-DSA. Under these conditions NH/CHα TOCSY signals of C13 are sensibly decreased in intensity, in particular in the region spanning from Ala^{6} to Ile^{13}. Conversely, as evident from the Figure 7D, NH/CHα TOCSY cross-peaks of C13 in the presence 16-DSA remain almost unmodified in their intensity, suggesting that C13 has no contact with the interior of the micelle structure. It is interesting to note that 5-DSA yields an evident decrease of signals relative to the last C13 C-terminal residues; on the contrary this effect is not observable in the case of LIPO-C13, revealing that in the absence of the hydrophobic tail the hydrophobic C-terminal residues, rather than the lipidic tail, have direct contact with the micelle.

To further investigate peptide positioning in micellar systems, we performed EPR measurements on DPC and SDS solutions, using 5-DSA and 16-DSA as spin-probes (*47*, *48*). For all the investigated signals, a triplet of narrow lines was obtained, indicating that the micellar environment in which the spin-probes are inserted present a quite dynamical structure, in which molecules' free tumbling is allowed. Table 2 contains the nitrogen coupling constant, indicative of microenvironment polarity, and the spin probe correlation time, indicative of microenvironment viscosity, for all the samples under consideration. The data show that in the presence of both peptides the mobility of the molecular probes decreases, thus increasing the correlation time. Meanwhile, the polarity experienced by the spin-probe remains unchanged, as highlighted by the constant values assumed by the nitrogen coupling constants. This evidence indicates a significant perturbation of the micelles' structure due to their interaction with the peptides. In the case of C13, this effect is found only with DPC and involves only the external layer of the micelle, since only the correlation time of 5-DSA increases, while that of 16-DSA seems unperturbed. In the case of LIPO-C13, the correlation time of both 5-DSA and 16-DSA changes, indicating that the perturbation extends to the micelles' interior.

DISCUSSION

CNP is a myelin-associated enzyme which *in vitro* specifically catalyzes the hydrolysis of 2′,3′-cyclic nucleotides to produce 2′-nucleotides. Although its main biological function is still unknown, numerous studies suggest a role for this protein in the migration and/or expansion of membranes during myelination (*2*). In particular CNP has recently proven to be necessary to anchor tubulin to the plasma membrane, thus assuming a possible role in all functions which require the association of tubulin to the membrane (*5*−*7*). The fragment responsible for CNP's binding to tubulin and, at same time, for CNP insertion into

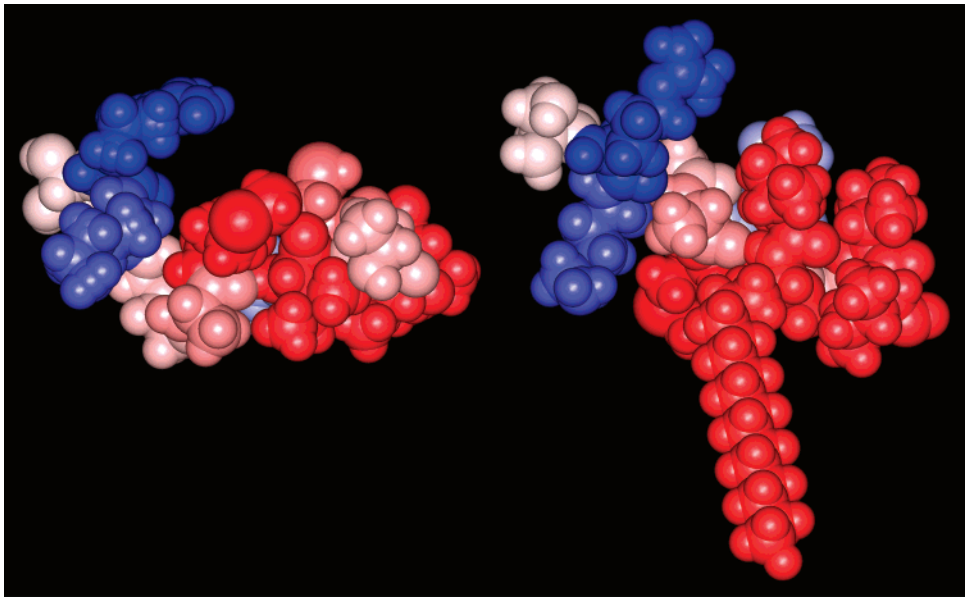

FIGURE 6: Van der Waals surface representation of C-13 (left) and LIPO-C13 (right) structures, obtained in DPC micelles. The surfaces are colored accordingly with a hydrophobic scale where polar charged, medium polar, or hydrophobic regions of the surface are colored blue, white, and red, respectively.

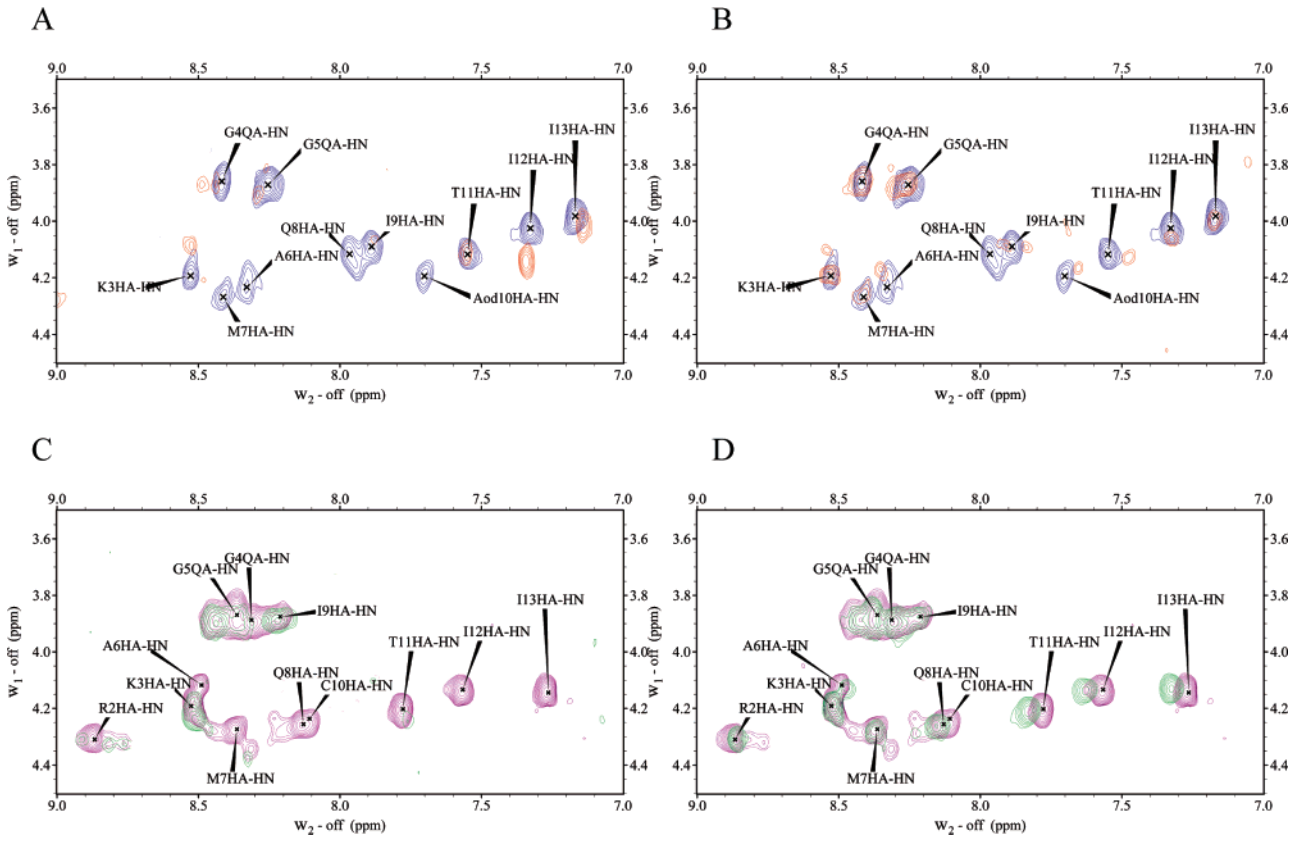

FIGURE 7: (A, B) Overlapping of the NH−CHα regions of TOCSY spectra relative to LIPO-C13 in DPC micelles recorded in the presence of 5-DSA (A) and 16-DSA (B) spin labels. (C, D) Overlapping of the NH−CHα regions of TOCSY spectra relative to C13 in DPC micelles, recorded in the presence of 5-DSA (C) and 16-DSA (D) spin labels.

the membrane consists of 13 amino acids. It is located in the C-terminal region of the protein and includes a consensus site CAAX for post-translational prenylation (*6*).

Post-translational modification and membrane targeting of CNP and other prenylated proteins have been studied in great detail (*2*, *11*). Palmitoylation, in combination with the CAAX-dependent modifications, targets proteins to the plasma membrane. The CAAX motif alone targets proteins to the endomembrane system, where they are proteolytically processed and methylated. Further trafficking of prenylated proteins to the plasma membrane is dependent on palmitoylation (*49*).

To date, the structural bases of the molecular interaction between prenylated proteins and plasma membrane, inde-

Table 2: Nitrogen Coupling Constant, $\langle A_N \rangle$, and Spin Probe Correlation Time, τ_C, Measured by EPR Experiments on C13 and LIPO-C13 in SDS and DPC Micelle Systems

	5-DSA		16-DSA	
	$\langle A_N \rangle$/G	$\tau_C \times 10^{11}$/s	$\langle A_N \rangle$/G	$\tau_C \times 10^{11}$/s
H_2O-DPC	14.8	2.8	15.0	1.1
H_2O-C13-DPC	14.7	3.9	15.0	1.2
H_2O-LIPO-C13 -DPC	14.6	4.2	14.8	2.0
H_2O-SDS	15.7	8.2	15.4	4.7
H_2O-SDS	15.6	8.6	15.2	5.0
H_2O-LIPO-C13-SDS	15.4	10.1	15.1	5.8

pendently of the post-prenylation process, is an unknown and uninvestigated topic. This study approaches this issue and suggests a model for the interaction of the C-terminal region of CNP, including the CAAX box, with the membrane; this model can also be of relevance for other prenylated proteins.

The peptide responsible for CNP insertion into the membrane, C13, and its lipidated derivative, LIPO-C13, were synthesized in our lab and structurally investigated by means of CD and high-resolution ^{1}H NMR spectroscopy, in membrane mimetic environments. As membrane mimetics, we chose micellar solutions of negatively charged SDS and zwitterionic DPC surfactants (*50*). To validate CD and NMR data using a more significant biomimetic system, CD data were recorded in DOPG and DOPC multilamellar vesicles.

The interaction of peptides with biological membranes depends on a fine equilibrium between electrostatic and hydrophobic forces. Charged or polar residues are generally involved in electrostatic interactions with the charged polar heads of membrane surfactants; on the other hand, the apolar amino acids and the lipophilic tails of surfactant molecules are in contact via hydrophobic interactions. Peptide insertion into the membrane, peptide membrane crossing, or poration, typical of cell penetrating peptides (CPPs) and of antimicrobic peptides (AMPs), are not fully understood processes driven, in a complex way, by hydrophobic and/or electrostatic interactions. Recently the concept of membrane potential perturbation (MPP) has been considering as a property that describes the membrane−peptide interaction from a structural viewpoint. It measures the potential of a peptide in attracting anionic lipids from the membrane, irrespective of the simple hydrophobic/electrostatic balance and of the specific structural scaffold underneath (*51*−*53*).

The lipidated peptide, LIPO-C13, in DPC zwitterionic micelle solution assumes a regular α-helical structure, with amino acid side chains occupying well defined conformational spaces (Figure 5B). In agreement with the secondary shifts of amide protons, the helix does not present an amphipathic character. On the contrary the observation of Van der Waals surfaces (Figure 6) indicate a large hydrophobic shell corresponding to the C-terminal portion of the molecule and a narrow, polar-charged region localized in the C-terminus of the peptide chain. EPR data show that a perturbation of the micelle system extending from the surface to the interior is recordable in DPC systems in the presence of LIPO-C13. Additionally the LIPO-C13 NMR spectrum is perturbed by the presence of both 5-DSA- and 16-DSA-labeled phospholipids. Accordingly, the large, hydrophobic C-terminal region of LIPO-C13 in DPC micelles is in close contact with the lipidic chains of the membrane phospholipids, confirming the possibility that this portion lies on the membrane surface, correctly positioned to direct the prenyl tail of Cys^{10} into the interior of the membrane structure (Figure 8A).

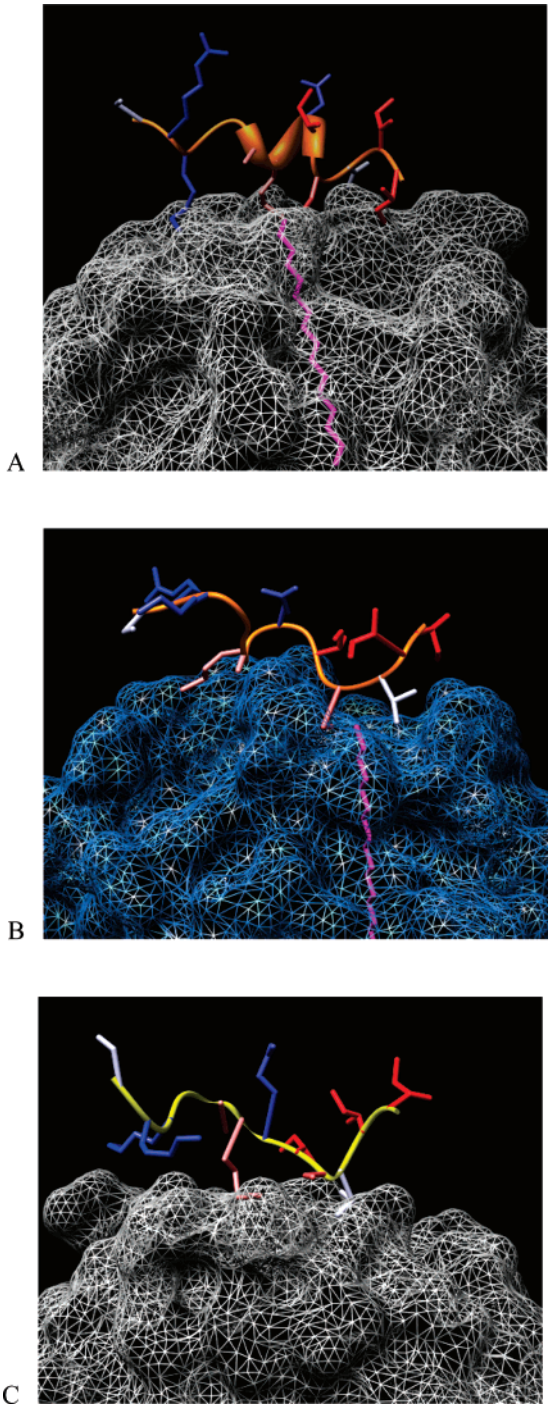

FIGURE 8: (A, B) NMR models of LIPO-C13 positioned on zwitterionic (A) and negative charged (B) membrane surfaces. (C) NMR model of C13 positioned on zwitterionic membrane surface. The lipidic tail colored in pink is inserted in the hydrophobic membrane. Apolar residues of the C terminus are colored in red-orange. Lys and Arg residues at the N-terminus are colored in blue.

LIPO-C13 in negatively charged SDS micelles exhibits only partially ordered structures as compared to LIPO-C13 in DPC. In this case a non-negligible electrostatic interaction should be considered because of the presence of the negative sulfate heads of SDS, which attract N-terminal Arg and Lys residues. The hydrophobic binding forces are

counterbalanced by the electrostatic forces which lead the peptide to assume less regular secondary structures. C13, although less regularly folded, presents its C-terminal portion in close contact with the membrane compartment (Figure 8B).

On the basis of the hydrophobic/electrostatic balance, we can explain the structural behavior of nonlipidated C13 in SDS and in DPC micelles. In the case of the nonlipidated C13 in zwitterionic DPC micelles, the hydrophobic contribution is reduced due to the absence of the lipidic tail; nevertheless the electrostatic contribution is also limited by the presence of the zwitterionic surface. Thus the hydrophobic interactions seem to have a slight prevalence, so that partial regular secondary structures of C13 at the C-terminus (Figure 8C) are promoted. CD and NMR data agree on the C13 assuming unfolded, extended conformations in a negatively charged SDS environment. Under these conditions both the hydrophobic and electrostatic binding forces enable C13 to interact with the micelle surface; consequently, the biomolecule assumes extended conformations out of the micellar compartment.

The CD data recorded for C13 and LIPO-C13 in SDS and DPC micelles are in agreement with the high-resolution NMR data. The CD spectra recorded in the presence of vesicles show a general preference of C13 and LIPO-C13 to assume turn-helical rather than random coil conformations. Thus, the structural stabilizing effect of the hydrophobic surface is confirmed even in more complex membrane-mimicking systems. Under these conditions the low intensity of C13 CD spectra in negatively charged DOPG vesicles confirms the NMR results on the weak tendency of the nonlipidated peptide to interact with the negatively charged membrane surface.

Our structural investigation performed on C13 and LIPO-C13 in the aforementioned micellar and vesicle systems defines structural pictures of different conditions of peptide/membrane interaction. These conditions are generated by modulating charge and hydrophobicity of the membrane mimetic system, on one side, and the properties of the peptide surfaces, on the other side. The amplification of the hydrophobic surface on LIPO-C13, due to the presence of the lipidic tail, along with the presence of a zwitterionic membrane surface defines optimal situations enabling the peptide to be regularly folded and correctly positioned on the membrane surface. Interestingly, in an opposite way, the importance of the hydrophobicity is emphasized by the conformational behavior of nonlipidated C13 in SDS negatively charged micelles. It is well known that the cell membrane has a very complex biological structure composed of many different biomolecules but carrying a final net negative charge (*54*). From a biological viewpoint, the poor tendency of C13, lacking a lipidic chain, to interact with negatively charged micelles and its preference for extended conformations emphasizes the role of the post-translational prenylation as indispensable to increasing, on a negative charged membrane, the hydrophobic molecular surface which favors the correct anchoring of the polypeptide to the membrane surface. This model can be generalized to many other amphitropic proteins such as Src kinase, Ras-guanine nucleotide exchange factor, protein kinase C, and cytidyl transferase, sharing with CNP the ability to migrate between the cytoplasm and the membrane for different functions (*55*−*57*). Our data provide a structural interpretation of the post-translational lipidation as a biomolecular trick to enlarge the hydrophobic surface and to enable the contact of the protein with the membrane. Interestingly, biological data on the role of post-prenylation processing of Rho proteins show that the presence of geranylgeranylation rather than farnesylation is crucial for the correct localization of the protein in the cell. Indeed, whereas the 20-carbon geranylgeranyl modification confers sufficient hydrophobicity to Rho proteins to allow them to associate with membranes and regulate effectors, the 15-carbon farnesyl modification is below the threshold for promoting membrane association (*58*).

Finally, it is interesting to analyze the binding of CAAX-prenylated proteins in comparison with the binding mode of other nonprenylated amphiprotic proteins which also have vital biological functions in association with the plasma membrane. In these cases the protein/membrane interaction is mediated by an amphipathic helix that include basic residues, which bind the protein to the membrane via electrostatic interactions; nevertheless, under these conditions, a consistent and essential contribution to the hydrophobic interaction is dependent on the presence of Phe, Trp, Tyr aromatic residues, which are well known to give a high interfacial hydrophobicity contribution to protein−membrane interaction (*59*, *60*).

SUPPORTING INFORMATION AVAILABLE

Chemical shift assignments and chemical shift indexes of C13 and LIPO-C13 in SDS and DPC micelles are available free of charge via the Internet at http://pubs.acs.org.

REFERENCES

1. Sprinkle, T. J. (1989) 2′,3′-Cyclic nucleotide 3′-phosphodiesterase, an oligodendrocyte-Schwann cell and myelin-associated enzyme of the nervous system, *CRC Crit. Rev. Neurobiol. 4*, 235−301.
2. De Angelis, D. A., and Braun, P. E. (1996) 2′,3′-Cyclic nucleotide 3′-phosphodiesterase binds to actin-based cytoskeletal elements in an isoprenylation-independent manner, *J. Neurochem. 67*, 943−951.
3. O' Neill, R. C., Minuk, J., Cox, M. E., Braun, P. E., and Gravel, M. (1997) CNP2 mRNA directs synthesis of both CNP1 and CNP2 polypeptides, *J. Neurosci. Res. 50*, 248−257.
4. De Angelis, D. A., Braun, P. E., Shtybel, W. W., and Bernier, L. (1991) Isoprenoid modification permits 2′,3′-cyclic nucleotide 3′-phosphodiesterase to bind to membranes, *J. Neurosci. Res. 30*, 540−544.
5. Lee, J., Gravel, M., Zhang, R., Thibault, P., and Braun, P. E. (2005) Process outgrowth in oligodendrocytes is mediated by CNP, a novel microtubule assembly myelin protein, *J. Cell Biol. 170*, 661−73.
6. Bifulco, M., Laezza, C., Stingo, S., and Wolff, J. (2002) 2′,3′-Cyclic nucleotide 3′-phosphodiesterase: a membrane-bound, microtubule-associated protein and membrane anchor for tubulin, *Proc. Natl. Acad. Sci.* U.S.A. *99*, 1807−1812.
7. Laezza, C., Wolff, J., and Bifulco, M. (1997) Identification of a 48-kDa prenylated protein that associates with microtubules as 2′,3′-cyclic nucleotide 3′-phosphodiesterase in FRTL-5 cells, *FEBS Lett. 413*, 260−264.
8. Simonds, W. F., Butrynski, J. E., Gautam, N., Unson, C. G., and Spiegel, A. M. (1991) Identification of a 48-kDa prenylated protein that associates with microtubules as 2′,3′-cyclic nucleotide 3′-phosphodiesterase in FRTL-5 cells, *J. Biol. Chem. 266*, 5363−5366.
9. Stephenson, R. C., and Clarke, S. (1990) Identification of a C-terminal protein carboxyl methyltransferase in rat liver membranes utilizing a synthetic farnesyl cysteine-containing peptide substrate, *J. Biol. Chem. 265*, 16248−16254.

10. Zhang, F. L., and Casey, P. J. (1996) Protein prenylation: molecular mechanisms and functional consequences, *Annu. Rev. Biochem. 65*, 241−269.
11. De Angelis, D. A., and Braun, P. E. (1994) Isoprenylation of brain 2′,3′-cyclic nucleotide 3′-phosphodiesterase modulates cell morphology, *J. Neurosci. Res. 39*, 386−397.
12. Cadwallader, K. A., Paterson, H., Macdonald, S. G., and Hancock, J. F. (1994) N-terminally myristoylated Ras proteins require palmitoylation or a polybasic domain for plasma membrane localization, *Mol. Cell Biol. 14*, 4722−4730.
13. Aller, S. G., Lombardo, I. D., Bhanot, S., and Forrest, J. N. (1999) Cloning, characterization, and functional expression of a CNP receptor regulating CFTR in the shark rectal gland, *Am. J. Physiol. 276*, 442−449.
14. Kelley, T. J., Cotton, C. U., and Drumm, M. L. (1997) In vivo activation of CFTR-dependent chloride transport in murine airway epithelium by CNP, *Am. J. Physiol. 273*, 1065−1072.
15. Butrynski, J. E., Jones, T. L. Z., Backlund, P. S., and Spiegel, A. M. (1992) Differential isoprenylation of carboxy-terminal mutants of an inhibitory G-protein alpha-subunit: neither farnesylation nor geranylgeranylation is sufficient for membrane attachment, *Biochemistry 31*, 8030−8035.
16. Drechsel, D. N., Hyman, A. A., Cobb, M. H., and Kirschner, M. W. (1992) Modulation of the dynamic instability of tubulin assembly by the microtubule-associated protein tau, *Mol. Biol. Cell 3*, 1141−1154.
17. Marta, C. B., Ortiz, E. H., Hallak, M., Baron, B., Guillou, F., Zakin, M. M., Soto, E. F., and Pasquini, J. M. (2002) Changes in the expression of cytoskeletal proteins in the CNS of transferrin transgenic mice, *Dev. Neurosci. 24*, 242−251.
18. Laezza, C., Notarnicola, M., Caruso, M. G., Messa, C., Macchia, M., Bertini, S., Minutolo, F., Portella, G., Fiorentino, L., Stingo, S., and Bifulco, M. (2006) N6-isopentenyladenosine arrests tumor cell proliferation by inhibiting farnesyl diphosphate synthase and protein prenylation, *FASEB J. 20*, 412−418.
19. Birnbaum, G., Kotilinek, L., Schlievert, P., Clark, H. B., Trotter, J., Horvath, E., Gao, E., Cox, M., and Braun, P. E. (1996) Heat shock proteins and experimental autoimmune encephalomyelitis (EAE): I. Immunization with a peptide of the myelin protein 2′,3′ cyclic nucleotide 3′ phosphodiesterase that is cross-reactive with a heat shock protein alters the course of EAE, *J. Neurosci. Res. 44*, 381−396.
20. Gravel, M., Peterson, J., Yong, V. W., Kottis, V., Trapp, B., and Braun, P. E. (1996) Overexpression of 2′,3′-cyclic nucleotide 3′-phosphodiesterase in transgenic mice alters oligodendrocyte development and produces aberrant myelination, *Mol. Cell Neurosci. 7*, 453−466.
21. Vlkolinsky, R., Cairns, N., Fountoulakis, M., and Lubec, G. (2001) Decreased brain levels of 2′,3′-cyclic nucleotide-3′-phosphodiesterase in Down syndrome and Alzheimer's disease, *Neurobiol. Aging 22*, 547−553.
22. Sloane, J. A., Hinman, J. D., Lubonia, M. W., and Abraham, C. R. (2003) Age-dependent myelin degeneration and proteolysis of oligodendrocyte proteins is associated with the activation of calpain-1 in the rhesus monkey, *J. Neurochem. 84*, 157−168.
23. Lappe-Siefke, S., Goebbels, M., Gravel, E., and Nicksch, J. (2003) Disruption of Cnp1 uncouples oligodendroglial functions in axonal support and myelination, *Nat. Genet. 33*, 366−374.
24. Muraro, P. A., Kalbus, M., Afshar, G., McFarland, H. F., and Martin, R. (2002) T cell response to 2′,3′-cyclic nucleotide 3′-phosphodiesterase (CNPase) in multiple sclerosis patients, *J. Neuroimmunol. 130*, 233−242.
25. Higuchi, M., Zhang, B., Forman, M. S., Yoshiyama, Y., Trojanowski, J. Q., and Lee, V. M. (2005) Axonal degeneration induced by targeted expression of mutant human tau in oligodendrocytes of transgenic mice that model glial tauopathies, *J. Neurosci. 25*, 9434−9443.
26. Roher, A. E., Weiss, N., Kokjohn, T. A., Kuo, Y. M., Kalback, W., Anthony, J., Watson, D., Luehrs, D. C., Sue, L., Walker, D., Emmerling, M., Goux, W., and Beach, T. (2002) Increased A beta peptides and reduced cholesterol and myelin proteins characterize white matter degeneration in Alzheimer's disease, *Biochemistry 41*, 11080−11090.
27. Lauterwein, J., Bosch, C., Brown, L. R., and Wüthrich, K. (1979) Physicochemical studies of the protein-lipid interactions in melittin-containing micelles, *Biochim. Biophys. Acta 556*, 244−264.
28. Opella, S. J., Kim, Y., McDonnell, P. (1994) Experimental nuclear magnetic resonance studies of membrane proteins, *Methods Enzymol. 239*, 536−560.
29. Whitmore, L., and Wallace, B. A. (2004) DICHROWEB, an online server for protein secondary structure analyses from circular dichroism spectroscopic data, *Nucleic Acids Res. 32*, 668−673.
30. Bader, R., Bettio, A., Beck-Sickinger, A. G., and Zerbe, O. (2001) Structure and dynamics of micelle-bound neuropeptide Y: comparison with unligated NPY and implications for receptor selection, *J. Mol. Biol. 305*, 307−329.
31. Killian, J. A., Trouard, T. P., Greathouse, D. V., Chupin, V., and Lindblom, G. (1994) A general method for the preparation of mixed micelles of hydrophobic peptides and sodium dodecyl sulphate, *348*, 161−165.
32. Braunschweiler, L., and Ernst, R. R. (1983) Interactions between Charged Polypeptides and Nonionic Surfactants, *J. Magn. Reson. 53*, 521−528.
33. Bax, A., and Davis, D. G. (1985) Mlev-17-based two-dimensional homonuclear magnetization transfer spectroscopy, *J. Magn. Reson. 65*, 355−360.
34. Macura, S., and Ernst, R. R. (1980) Elucidation of cross relaxation in liquids by two-dimensional NMR spectroscopy, *Mol. Phys. 41*, 95−117.
35. Jeener, J., Meyer, B. H., Bachman, P., and Ernst, R. R. (1979) Investigation of exchange processes by two-dimensional NMR spectroscopy, *J. Chem. Phys. 71*, 4546−4553.
36. Goddard, T. D., and Kneller, D. G. (2001) Measurement of H2′-C2′ and H3′-C3′ dipolar couplings in RNA molecules, SPARKY 3 NMR software, University of California, San Francisco.
37. Tedeschi, A. M., Franco, L., Ruzzi, M., Paduano, L., Corvaja, C., and D'Errico, G. (2003) Micellar aggregation of alchyltrimetilammonium bromide surfactants studied by electron paramagnetic resonance of an anionic nitroxide, *Phys. Chem. Chem. Phys. 5*, 4204−4209.
38. Guntert, P., Mumenthaler, C., and Wüthrich, K. (1997) Torsion angle dynamics for NMR structure calculation with the new program DYANA, *J. Mol. Biol. 273*, 283−298.
39. Case, D. A., Pearlman, D. A., Caldwell, J. W., Cheatham, T. E., III, Ross, W. S., Simmerling, C. L., Darden, T. A., Merz, K. M., Stanton, R. V., Cheng, A. L., Vincent, J. J., Crowley, M., Ferguson, D. M., Radmer, R. J., Seibel, G. L., Singh, U. C., Weiner, P. K., and Kollman, P. A. (1997) *AMBER 5*, University of California, San Francisco.
40. MSI Molecular Simulations, San Diego, California 92121−3752.
41. Wüthrich, K. (1986) *NMR of Proteins and Nucleic Acids*, John Wiley & Sons, New York.
42. Bruix, M., Parello, M., Herranz, J., Rico, M., and Nieto, J. L. (1990) Correlation of three-dimensional Structures with the antibacterial activity of a group of peptides designed ased on a nontoxic bacterial membrane anchor, *Biochem. Biophys. Res. Commun. 167*, 1009−1014
43. Wishart, S, D., Sykes, D, B., and Richards, F. M. (1992) The chemical shift index: a fast and simple method for the assignment of protein secondary structure trough NMR spectroscopy, *Biochemistry 31*, 1647−1651.
44. Koradi, R., Billeter, M., and Wuthrich, K. (1996) MOLMOL: a program for display and analysis of macromolecular structures, *J. Mol. Graphics 14*, 51−55.
45. Jarvet, J., Zdunek, J., Damberg, P., and Graslund, A. (1997) Three-dimensional structure and position of porcine motilin in sodium dodecyl sulfate micelles determined by ^{1}H NMR, *Biochemistry 36*, 8153−8163.
46. Lindberg, M., Jarvet, J., Langel, U., and Graslund, A. (2001) Secondary structure and position of the cell-penetrating peptide transportan in SDS micelles as determined by NMR, *Biochemistry 40*, 3141−3149.
47. Mendz, G. L., Moore, W. J., Kaplin, I. J., Cornell, B. A., Separovic, F., Miller, D. J., and Brown, L. R. (1988) Characterization of dodecylphosphocholine/myelin basic protein complexes, *Biochemistry 27*, 379−386.
48. Kang, Y. S., and Kevan, L. (1994) Interaction of Poly(ethylene oxide) with the Sodium Dodecyl Sulfate Micelle Interface Studied with Nitroxide Spin Probes, *J. Phys. Chem. 98*, 7624−7627.
49. Braun, P. E., De Angelis, D., Shtybel, W. W., and Bernier, L. (1991) Isoprenoid modification permits 2′,3′-cyclic nucleotide 3′-phosphodiesterase to bind to membranes, *J. Neurosci. Res. 30*, 540−544.
50. Esposito, C., D'Errico, G., Armenante, M. R., Giannecchini, S., Bendinelli, M., Rovero, P., and D'Ursi, A. M. (2006) Physicochemical characterization of a peptide deriving from the glycoprotein gp36 of the feline immunodeficiency virus and its

lipoylated analogue in micellar systems, *Biochim. Biophys. Acta 1758*, 1653−1661.
51. Zorko, M, Langel, U (2005) Cell-penetrating peptides: mechanism and kinetics of cargo delivery, *Adv. Drug Del. Rev. 57*, 529−545.
52. Wang, G., Li, Y., and Li, X. (2005) Correlation of three-dimensional structures with the antibacterial activity of a group of peptides designed based on a nontoxic bacterial membrane anchor, *J. Biol. Chem. 280*, 5803−5811.
53. Li, X., Li, Y., Peterkofsky, A., and Wang, G. (2006) NMR studies of aurein 1.2 analogs, *Biochim. Biophys. Acta 1758*, 1203−1214.
54. Yoon, Y, T., Jeong, C., Lee, S. W., Kim, J. H., Choi, M. C., Kim, S. J., Kim, M. W., and Lee, S. D. (2006) Topographic control of lipid-raft reconstitution in model membranes, *Nat. Mater. 5*, 281−285.
55. Burn, P. (1988) Amphitropic proteins: A new class of membrane proteins, *Trends Biochem. Sci. 13*, 79−83.
56. Johnson, J. E., and Cornell, R. B. (1999) Amphiprotic proteins Regulation by reversible membrane interactions, *Mol. Membr. Biol. 16*, 217−235.
57. Wang, G., Keifer, P. A., and Peterkofsky, A. (2003) Solution structure of the N-terminal amphitropic domain of Escherichia coli glucose-specific enzyme IIA in membrane-mimetic micelles, *Protein Sci. 12*, 1087−1096.
58. Wright, L. P., and Philips, M. R. (2006) Thematic review series: Lipid Posttranslational Modifications CAAX modification and membrane targeting of Ras, *J. Lipid Res. 47*, 883−891.
59. Wimley, W. C., and White, S. H. (1996) Experimentally determined hydrophobicity scale for proteins at membrane interfaces. *Nat. Struct. Biol. 10*, 842−848.
60. Karplus, P. A. (1997) Hydrophobicity regained, *Protein Sci. 6*, 1302−1307.

BI701474T